



# Geochemical interactions at the steel-bentonite interface caused by a hydrothermal gradient

Carlos Mota-Heredia<sup>a</sup>, Jaime Cuevas<sup>a</sup>, Ana I. Ruiz<sup>a</sup>, Almudena Ortega<sup>a</sup>, Elena Torres<sup>b</sup>,  
María Jesús Turrero<sup>b</sup>, Raúl Fernández<sup>a,\*</sup>

<sup>a</sup> Department of Geology and Geochemistry, Faculty of Sciences, Autonomous University of Madrid, Cantoblanco, 28049 Madrid, Spain

<sup>b</sup> CIEMAT, Av. Complutense 40, 28040 Madrid, Spain

## ARTICLE INFO

### Keywords:

Deep geological repository  
Bentonite  
Bentonite-iron interaction  
Hydrothermal gradient

## ABSTRACT

Bentonites are used in deep geological disposal facilities as an engineered barrier to isolate high level radioactive waste, contained in metallic canisters. The present study, performed at laboratory scale, evaluated the behaviour of MX-80 (Na-bentonite) and FEBEX (Ca-Mg-Na-bentonite) in contact with carbon steel, subjected to a hydrothermal gradient. A dominant Na-Cl-SO<sub>4</sub> saline solution was injected towards the compacted bentonite from the top, while a heater, located at the bottom in contact with the steel disc, maintained a constant temperature of 100 °C. The cells were studied after one and six months of interaction. Changes in the physical (water content and specific surface area) and chemical (cation exchange capacity and element distribution) properties of the bentonite were observed, as well as the formation of a corrosion layer on the steel, at the interface with bentonite, mainly composed of magnetite, maghemite and hematite. The bentonites were mainly altered at the mm scale, being enriched in iron content, and changing their ion distribution to Ca-dominant smectite (in MX-80 bentonite).

## 1. Introduction

High Level Radioactive Wastes (HLRW) must be isolated from the biosphere for many years until the radionuclides decay to reach natural background levels ( $>10^5$  years). Deep Geological Repositories (DGR) are the most accepted long-term option for isolating HLRW (Brookins, 1984; Chapman, 2006; El-Showk, 2022; IAEA, 2022).

The DGR concept consists of Engineered Barrier Systems (EBS), where HLRW are encapsulated within metallic canisters. The canister in most international concepts, is surrounded by a barrier of compacted bentonite blocks that protects the HLRW from groundwater infiltration, providing mechanical stability and buffering potential radionuclide leakage from the canister when it deteriorates (Villar and Lloret, 2004). The EBS might be emplaced in either crystalline hard rocks, evaporites or sedimentary rock formations. For structural support and seal of galleries, concrete will also be part of the EBS (Hedin, 1997; Bildstein and Claret, 2015; Norris, 2017; Marsh et al., 2021).

Carbon steel is one of the materials chosen to manufacture the metallic canisters that encapsulate the HLRW and gives them mechanical strength. Countries such as Switzerland, France, Japan, Belgium or

Spain have chosen this material for the manufacture of their canisters (ENRESA, 1997; Patel et al., 2012; NUMO, 2013; ONDRAF/NIRAS, 2013; Necib et al., 2016). In the Spanish DGR concept, ENRESA, the official agency responsible for nuclear waste management, has chosen the carbon steel TStE355 EN 10028-3 (ENRESA, 1997). In addition to lower costs, some studies demonstrate the good properties of carbon steel over copper or stainless steel for the manufacture of long-lived containers to be disposed of in a HLRW repository because of their long working life (over thousands of years) and predictable corrosion processes (Smailos and Kienzler, 2005; Torres Álvarez, 2011; Patel et al., 2012).

Bentonites are known for their good mechanical and chemical properties such as high swelling capacity due to their expansivity when incorporating water molecules, having a high water caption and cation retention capacity, as well as low permeability, high plasticity, radionuclide sorption, etc. (Villar, 2002; Gómez-Espina and Villar, 2010). This type of clay is mainly composed of montmorillonite, a type of smectite, plus accessory minerals.

Depending on the hydrogeological nature of the host rock, the groundwater in an EBS that can reach the bentonite will have different

\* Corresponding author.

E-mail address: [raul.fernandez@uam.es](mailto:raul.fernandez@uam.es) (R. Fernández).

<https://doi.org/10.1016/j.clay.2023.106984>

Received 30 January 2023; Received in revised form 5 May 2023; Accepted 8 May 2023

Available online 12 May 2023

0169-1317/© 2023 The Author(s). Published by Elsevier B.V. This is an open access article under the CC BY-NC-ND license (<http://creativecommons.org/licenses/by-nc-nd/4.0/>).

concentrations of soluble ions. Frequently, relative high concentrations ( $>0.1$  M in ion strength) characterize clay formations (Turrero et al., 2006; Mäder, 2009a, 2009b; Wersin et al., 2016; Gautschi, 2017) and low concentrations (low salinity) characterize granitic formations (Edmunds and Savage, 1991; Gómez et al., 2006; Garralón et al., 2017). It is also possible to find high salinity waters similar to seawater in the case of DGRs located at the coast, such as the Finnish (Hellä et al., 2014; Navarro et al., 2017) and Swedish disposal concepts (Laaksoharju et al., 1999; Ragvald, 2018).

Compacted bentonite blocks are installed in most DGR concepts as confining material. Usually, the placement is carried out under unsaturated conditions. The water in the host rock will hydrate the bentonite blocks from the outside while the radioactive waste will heat the bentonite from the surface of the canister. Under these conditions, the bentonite will undergo a hydrothermal gradient as the temperature will decay from the inner contact with the canister containing the HLRW towards the host rock and will hydrate in the opposite direction, from the outer host rock towards the canister. DGR concepts envisaged a maximum temperature of  $100\text{ }^{\circ}\text{C}$  at the canister surface to maintain the integrity of the bentonite (SKB, 2006), but higher temperatures are being considered more recently in order to enable larger quantities of HLRW containers per gallery. The rationale is to reduce the space, packaging, transport operations and other aspects to, consequently, reduce costs (Villar et al., 2020); although thermal engineering of the bentonite buffer to mitigate long-term thermal pressurization stresses in host rock should be fixed (Rutqvist, 2020).

The interaction between the metal canister and the bentonite barrier generates corrosion on the canister surface, influenced mainly by the high temperature, the porewater chemistry of bentonite (specially the pH and the concentration of chlorides, sulphur species and carbonates), the redox conditions and the degree of saturation (King and Shoesmith, 2010). Corrosion product layers of magnetite, ferric (oxyhydr)oxides (hematite, goethite lepidocrocite) and siderite in steel-clay environments have been identified at a mm scale in large in situ experiments after long timescales (FEBEX experiment at the Grimsel Test site, Switzerland, and ABM at the Äspö Hard Rock Laboratory, Sweden), representative of repository conditions (Necib et al., 2017; Kaufhold et al., 2018; Hadi et al., 2019; Wersin et al., 2021). Additionally, Mg anomalies and sulphates concentration at the steel-clay interface has been observed primarily attributed to the temperature gradient (Wersin et al., 2021). Kaufhold et al. (2013) described enrichment in Mg with formation of trioctahedral minerals/domains in some bentonites of the ABM experiment performed in Äspö, Sweden. This was later identified by Svensson (2015) as saponite for the FEBEX bentonite.

The steel-bentonite interaction may also produce precipitation of carbonates (mainly calcite) due to cation exchange of Ca by Mg or Fe ions in the short-term. Besides, accessory silica minerals (i.e. cristobalite, quartz) or montmorillonite dissolution in the long-term drive to the formation of Fe-silicates such as nontronite and cronstedtite (Chaparro et al., 2021).

Alteration of smectite, experimentally observed in low water/solid ratios experiments and low temperatures ( $< 50\text{ }^{\circ}\text{C}$ ), was relatively low, although irregularly distributed diffusion of Fe was found according to the water saturation of the bentonite and  $\text{Fe}^{\text{II}}/\text{Fe}^{\text{III}}$  distribution, depending of the varying redox conditions (Hadi et al., 2019). Mineral transformations of smectites in claystones and bentonite, induced by the metallic iron corrosion, have been reported to have different pathways with the rise of temperature. Over  $50\text{--}150\text{ }^{\circ}\text{C}$ , relevant to DGR environments, the formation of iron-rich serpentine-type minerals was commonly observed, whereas higher temperatures ( $150\text{--}300\text{ }^{\circ}\text{C}$ ) produced the formation of tri-octahedral iron-rich smectites as saponite (Guillaume et al., 2004; Mosser-Ruck et al., 2010, 2020; Lanson et al., 2012). As a consequence of corrosion and mineralogical changes, diffusion of  $\text{Fe}^{\text{II}}$  into the bentonite structure, changes in porosity and physico-chemical properties such as the cation exchange capacity or mechanical properties (e.g. decrease of swelling properties) have been

observed in high water/solid ratio laboratory experiments and observed minerals were predicted by modelling studies (Bildstein et al., 2006; Wilson et al., 2015; Wilson, 2017).

Bentonites with distinct smectite component seems to perform differently under the same experimental conditions of interaction with iron, although there were environmental reasons argued to explain such behaviour as pH or smectite/water ratio. Bentonites containing high charge smectites were found less corrosive than bentonites containing low charge smectites. Na-bentonites were found also less corrosive than Ca-bentonites (Kaufhold et al., 2015; Hadi et al., 2019). This source of variability must be checked with other bentonites to be able to state this behaviour with certainty.

The present study aims to advance in the knowledge on carbon steel-bentonite interaction under hydrothermal conditions using well-known compacted bentonites hydrated and heated ( $100\text{ }^{\circ}\text{C}$ ) from opposite directions. For this purpose, laboratory scale experiments have been performed (for 1 and 6 months) using two different bentonites, considered as reference buffer materials in DGR concepts: FEBEX (Ca-Mg-Na-bentonite, high charge montmorillonite) and MX-80 (Na-bentonite, low charge montmorillonite).

The methodological approach has been designed to provide information on the differences in corrosion depending on the bentonite used, prepared as it is intended to use in the repository. The measurement of physical-chemical properties and mineralogy along the hydrothermal gradient and the steel-bentonite interface allowed us to discuss the different impact of characteristic geochemical alteration of these critical material interfaces evolving in an active HLW repository.

## 2. Materials and methods

### 2.1. Experimental setup

Bentonite blocks were prepared from homogeneous bentonite powder with its natural moisture content. The dimensions of the cylindrical blocks are 21 mm in height and 50 mm in diameter, and they were uniaxially compacted to a dry density of  $1.65\text{ g}\cdot\text{cm}^{-3}$ . Each bentonite block was weighed before being placed in the cell with a mass of 76.9 g for FEBEX bentonite and 72.9 g for MX-80 bentonite. These amounts were calculated from the natural moisture content of each bentonite stored in the laboratory, being 12.5% and 7.2% respectively, to prepare a compacted block to the above specifications.

There was a minimum gap ( $<0.5$  mm) between the bentonite block and the cylindrical inner walls of the cell to be able to place the bentonite inside without any mechanical stress. In order to seal this gap, the bentonite blocks sat in their cells and were left to hydrate in a sealed chamber at 100% relative humidity, so that the bentonite swelled, adapting itself to the exact dimension of the cell and thus preventing the hydration solution to move preferentially from the lateral inner walls. The calculated dry density lies within the range  $1.50\text{--}1.57\text{ g}\cdot\text{cm}^{-3}$  before the initiation of the experiments.

The tests were performed using in-house designed hydrothermal cells (Fig. 1). The design of these cells was modified from those used previously by Martin et al. (2000), although the same concept of establishing a hydrothermal gradient prevailed. The cells were made of Teflon, with 25% glass fibre to improve their strength and dimensional stability. A stainless-steel outer ring wrapped the Teflon cell avoiding possible deformation due to the potential swelling pressure of the bentonites achieved with the hydration. A carbon steel disc was placed in contact with a stainless-steel plate, located at the bottom of the cell, containing a heating element and a temperature sensor, which acted as a heater. The temperature at the heater was automatically controlled by a sensor and recorded with a computer software throughout the whole duration of the experiments. A porous sintered stainless steel plate was placed on top of the bentonite, through which the hydration solution was homogeneously distributed. The hydration solution was injected to the bentonite block at low pressure from a small reservoir located at the

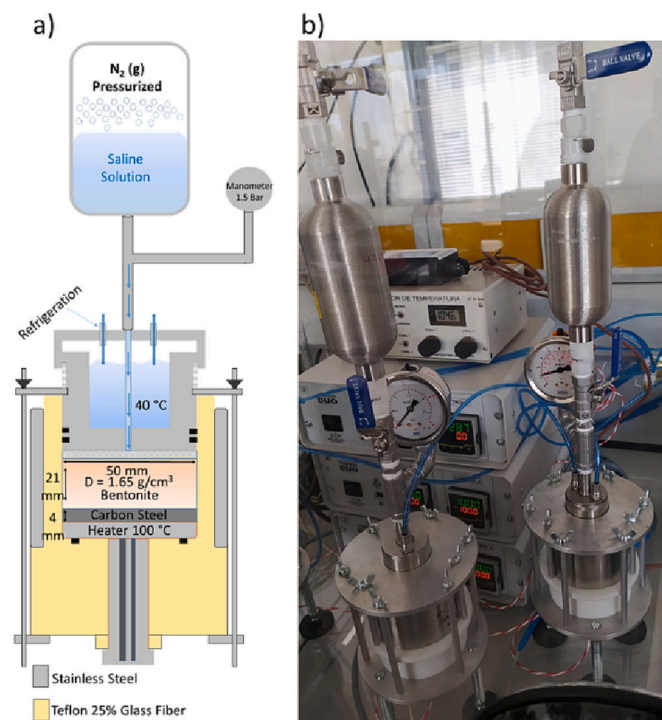


Fig. 1. a) Scheme of a hydrothermal cell, and b) Photograph of the experimental set-up showing two cells and the electronic temperature controls at the back.

top of the cell. The aim of the infiltration was to maintain a permanent available hydration throughout the whole duration of the experiments that maintained the hydrothermal gradient along the cell. Therefore, an initial infiltration pressure of 1.5 bar was supplied to the hydration solution tank from a nitrogen gas tank. When the flow switching valve located between the infiltration tank and the bentonite column was open, the infiltration pressure decreased but remained constant for each experiment within the range of 1.5 to 0.4 bar. To create a temperature gradient along the bentonite column, a water circuit was recirculated for cooling at the top side of the cell, maintaining a constant temperature at the hydration-bentonite interface. Once the thermal gradient equilibrium was reached, the carbon steel plate was at 100 °C while the upper part of the bentonite was at 40 °C.

Manipulation of samples (e.g. compaction and hydration of bentonites in the Teflon cells, preparation of the saline solution) before the start of each experiment was performed under atmospheric conditions, therefore, aerobic conditions prevailed at the beginning of the experiments until cells were closed and heaters were turned on.

Although the system was presumed closed, all experiments were carried out in a glove box in inert nitrogen atmosphere. This enabled the dismantling of the cells within the box, preventing oxidation and carbonation of samples with atmospheric oxygen and CO<sub>2</sub>, respectively. Once dismantled, the samples were embedded in a bicomponent transparent epoxy resin Araldite 2020™ with low viscosity to avoid the deformation and dehydration of bentonite and the exposure to atmospheric oxygen. The embedded samples were cured at room temperature, left in the chamber until the resin piece embedding the carbon steel-bentonite cylinders was hard and suitable for cutting and segmentation immersed in an oil cutting fluid.

## 2.2. Hydration solution

A bibliographic search of the data collected on the main components of the aqueous chemistry of the porewaters of the clayey formations Boom Clay (Belgium) (ONDRAF/NIRAS, 2013), Callovo-Oxfordian

(France) (Vinsot et al., 2008), Opalinus clay (Switzerland) (Mäder, 2009b) and a Paleogene continental mudrock (Spain) (Turrero et al., 2006) indicated that porewater types and concentrations can be very heterogeneous, even in different locations and depths of the same formation. In any case, all these porewaters have a dominant composition of sodium chloride with a very variable composition of sulphate and significant amounts of calcium and magnesium. These ions come from the equilibrium between the clay mineralogy of each formation and the water. All three clay formations contain water-soluble minerals such as carbonates, sulphates and chloride salts. The chemical composition of the porewaters is controlled by processes such as ion exchange reactions and solubility reactions modified locally by diffusive transport. The high sulphate concentration can be explained by the presence of accessory minerals such as gypsum and celestite, and the oxidation reaction from pyrite (Pearson et al., 2011; Wersin et al., 2016).

These interactions are controlled by parameters such as porosity, pH, solubility constraints, microorganisms activity, redox reactions, etc. (Gaucher et al., 2006; Beaucaire et al., 2012).

For the present study, a synthetic saline porewater solution representative of a generic clay formation was used. For this purpose, a dominant Na-Cl-SO<sub>4</sub> type solution was prepared with the following measured chemical composition (ions in mM): 38.9 Cl<sup>-</sup>, 13.8 SO<sub>4</sub><sup>2-</sup>, 3.3 HCO<sub>3</sub><sup>-</sup>, 44.8 Na<sup>+</sup>, 1.8 K<sup>+</sup>, 7.5 Ca<sup>2+</sup> and 5.1 Mg<sup>2+</sup> and pH = 7.9, a value that was the result of the solution equilibrium under atmospheric conditions. The calculated error in the charge balance for this solution after being synthesized in the laboratory was <2%.

## 2.3. Carbon steel

The material selected to isolate the HLRW in the Spanish concept is the TStE 355 carbon steel (ENRESA, 1997). This material is mainly Fe (>97 wt%) with small quantities of C, Cr, Mo and Mn.

Each carbon steel plate was cleaned with ethanol, to remove any potential organic contamination from the metallic surface, and weighed before being placed in the cell. A porous steel plate was placed on top of the compacted bentonite to maintain the integrity of the bentonite and to distribute the infiltration solution homogeneously. The porous steel plates were also cleaned with ethanol.

## 2.4. Bentonite

To carry out this study two bentonites were used, MX-80 and FEBEX.

MX-80 is Na-bentonite from Wyoming (USA), considered as a reference buffer and backfill material for the disposal of radioactive waste by several countries and has been extensively studied in this context (Bradbury and Baeyens, 2003, 2009; Montes-H et al., 2005; Jönsson et al., 2009). An in-house mineralogical quantification achieved by coupling a Rietveld refinement using SIROQUANT® and selective chemical determination and extraction of readily soluble silica and calcite (described in Cuevas et al., 2022) revealed that the selected material contains 87 ± 1% montmorillonite, 4% quartz, 3% cristobalite, 2% K-feldspar and plagioclases and other minerals such as micas and calcite in minor content. Traces of goethite, magnetite and pyrite were also present. The cation exchange capacity (CEC) is 75 ± 4 cmol(+)·kg<sup>-1</sup> determined by the Cu(II)-triethylenetetramine method (Cu-trien), and the specific surface area (SSA) determined by Brunauer, Emmett and Teller (BET) analysis is 23 ± 2 m<sup>2</sup>·g<sup>-1</sup>. Its initial water content in the present study was 7.2%.

FEBEX bentonite was extracted from the Cortijo de Archidona, in Serrata de Níjar, Almería, Spain (Caballero et al., 1983, 2005; Fernández et al., 2004). It is the reference buffer material for disposal of radioactive waste in Spain (ENRESA, 1998). According to Cuevas et al. (2022) this is a Ca-Mg-Na-bentonite, composed by 85 ± 2% of montmorillonite, 4% quartz, 4.5% cristobalite, <1% K-feldspars, 5% plagioclases, and 0.8% calcite and other trace minerals including goethite and magnetite. A relative 10% error should be considered for several performed



quantifications. The cation exchange capacity is  $94 \pm 1 \text{ cmol}(+)\cdot\text{kg}^{-1}$  determined by the Cu-trien method and the specific surface area, determined by BET analysis, is  $50 \pm 5 \text{ m}^2\cdot\text{g}^{-1}$ . Its initial water content in the present study was 13.0%.

## 2.5. Sample segmentation after experiments

Two columns (1-month experiments) were cut using the Well 4240 diamond wire saw from Well Diamond Wire Saws. To preserve the samples from atmospheric oxygen, cuts and sampling were carried out in a glove box with an inert nitrogen atmosphere. The two other columns (6-month experiments) were cut with the Secotom-6 saw machine from Struers™, using a cooling oil that do not interact with the sample and preserve it from the atmospheric oxygen. The diamond wire cutting systems preserved an optimal amount of bentonite sample as the cut was smooth and the wire diameter  $< 0.5 \text{ mm}$  but the cutting resin and steel parts was a very time-consuming process, and maintaining a low oxygen atmosphere was difficult. Therefore, using a saw machine was a much faster and safer option for preserving the sample. None of the two methods heated the samples while cutting and both had advantages and disadvantages but, in general, the Secotom-6 saw was preferred for the longitudinal cuts on cylindrical steel-bentonite samples and the diamond wire transversal bentonite cuts, parallel to the steel-bentonite interface. To study the reactivity along the hydrothermal gradient, samples were cut to provide enough material for each characterization technique, according to the scheme shown in Fig. S1 (see in supplementary material).

## 2.6. Analytical methods

The following bulk physical-chemical characteristics was characterised in different sections of bentonite from the steel-bentonite interface: geotechnical water content, BET SSA and CEC. The characterization of the impact of steel corrosion in bentonite was studied through SEM-EDX chemical profiles and detailed interface observations complemented by the study of XRD powder patterns regarding localized zones including steel-bentonite interface.

Water content was measured by mass difference after heating to constant weight at  $105^\circ\text{C}$ .

The determination of the SSA was performed by nitrogen adsorption using a Gemini V analyzer from Micrometrics and calculated by the BET method. The samples were ground and dried at  $90^\circ\text{C}$  for 24 h. Then, the samples were degassed at  $90^\circ\text{C}$  for at least 1 h using a nitrogen gas stream, and finally analysed in the equipment using the 5-points isotherm method as in Cuevas et al. (2016).

The CEC was measured by triplicate for each sample using the Cu-trien method (Meier and Kahr, 1999), following the modifications performed in the method for clays by Ammann et al. (2005). Wet samples were grinded with an agate mortar, placed in Cu-trien suspension, dispersed, and then centrifuged. The measurement of absorbance at 577 nm of the aqueous phase were performed using the UV-Visible Spectrophotometer Genesys 150 by Thermoscientific. CEC measurements were corrected according to the water content determined for each sample.

The cut and segmented sections (paragraph 2.4) were prepared for scanning electron microscope (SEM) and energy-dispersive X-ray (EDX) analyses. The following sequence was performed to prepare each sample: the water content in the bentonite samples was removed by immersion of the sample in liquid nitrogen during 30 min followed until pressure decreases below  $10^{-6}$  Torr, typically after 3 days (in house freeze drying method). Once dried, the samples were embedded again in Araldite 2020™ resin to obtain rigid pieces that could be cut with the saw. Afterwards, the samples were polished with sandpaper of different grain sizes until flat surfaces, suitable for microscopic studies, were achieved. The steel-bentonite interfaces must be well preserved as the alteration in these zones are expected in a very narrow extension.

Careful polishing needs to be performed since the hardness of steel and compacted bentonite are very different and both materials must be polished together. Finally, samples were coated by Au sputtering with a Q150T-S Quorum sputter coater system.

The images of surface and morphologies were taken with a Hitachi S-3000 N SEM coupled to a EDX XFlash® 6130 Bruker detector for semi-quantification analyses of chemical composition. The EDX quantification was performed by means of internal standard quantitative analyses. The equipment operates under high vacuum conditions using an accelerating voltage of 20 keV, lifetime of 40 s, a working distance from 15.0 to 18.5 mm and a beam current of 300 mA.

The analyses started with a scanning along the interface taking images and EDX analyses of the carbon steel, the bentonite and their interaction, to have an estimation of the crust thickness. Then, an area was chosen for the study of the longitudinal profile of chemical composition, in the direction from the heater to the hydration zone. The magnification of the images was higher at the steel-bentonite interface and hydration zone than at the medium zone of bentonite, where the chemical variations were expected to be less significant. Approximately 40 analyses were performed over a thickness of 2 mm at the steel-bentonite interface; 20 analyses were performed over a thickness of 3 mm at the hydration zone and 40 analyses were performed at the intermedium zone over a thickness of 16 mm, although the number of analyses and thickness may slightly vary from one sample to other. The EDX analyses were studied to observe the diffusion of Fe along the bentonite and concentration changes of elements such as Mg, Ca, Na, K, Cl and S. The data were treated by removing C and O and recalculated as a percentage by weight. The mineralogy at the steel-bentonite interface was also analysed on fresh fractured samples at both sides, with the objective to observe morphologies of the reaction products. Small samples that either fell apart or were manually separated were used for this study.

X-Ray Diffraction (XRD) was used to study the mineralogical changes along the bentonite block and at the interface with steel. The analyses were performed using a Bruker D8 Discover diffractometer with a Ge monochromator and a lynxeye XE-T fast detector. The patterns were measured in a range of  $3\text{--}70^\circ 2\theta$ , with angular increments of  $0.02^\circ$  and times of 1 s. The device operated at 40 kV and 40 mA. For the samples taken near to the interface ( $<1 \text{ mm}$  from the heater) and the crust formed between the steel and bentonite, an airtight holder (Fig. 2) that preserved the samples from the atmospheric oxygen was used, avoiding the oxidation of possible reduced compounds. The sample of bentonite was measured in powder and the crust was directly analysed as a sheet. The identification of mineral phases in X-ray diffractograms was performed by using the software X'Pert HighScore Plus® of PANalytical™. The use of the airtight holder produced an increase of signal to noise background ratio and prevented us to try a refinement basis quantification due to the poor quality of the registered patterns.



**Fig. 2.** Sample collection for XRD: a) aspect of MX-80 section after cutting; b) airtight holder to isolate from atmospheric oxygen; c) crust of steel/bentonite interface of MX-80 after 6 months for XRD analysis.



### 3. Results

#### 3.1. Physical-chemical characterization

##### 3.1.1. Water content and SSA

The water content in the experiments performed with MX-80 bentonite increased from 7 to 18 wt% after 1 month, while after 6 months the block was fully saturated at ~30–33 wt% (Fig. 3a). The SSA measurements show heterogeneous results along the bentonite block. At the interface this property decreased considerably due to the presence of corrosion products after only 1 month. After 6 months the decrease was even larger. It was observed that with the increasing time the SSA decreased near the hydration zone and the decrease was larger with the increasing reaction time. Only in the centre of the bentonite block the SSA was observed to remain in similar values as in the initial stage or even higher.

The FEBEX samples slightly increased in the water content from 13% to ~17% after 1 month, but it did not have a further increase after 6 months (Fig. 3b). SSA analyses were not performed after 1 month, but after 6 months the results were similar to the reference bentonite, except for the closest zone to the interface, where the SSA decreased from ~50 to 24 m<sup>2</sup>·g<sup>-1</sup>. In any case, near the steel-bentonite interface, the SSA decreased significantly due to the formation of the cemented crust of corrosion products, in agreement with the SEM observations.

##### 3.1.2. CEC

The CEC in MX-80 decreased after 1 month except in the medium zone (sample representative of a thickness between 6 and 15 mm) of the bentonite column and remained almost constant near the original values after 6 months of reaction in all samples, with even higher values than in the original bentonite in the region close to the interface with steel. In the case of the FEBEX bentonite samples, the CEC decreased around 5% after 1 month and more after 6 months, although, again at the medium zone the CEC was slightly lower than after 1 month (Table 1). It might be considered that the standard deviations calculated for these measurements were relatively high, so that these results should indicate only a general trend.

#### 3.2. EDX chemical profiles and mineralogical characterization

SEM-EDX analyses along the MX-80 bentonite column showed that

**Table 1**

CEC [cmol(+)/Kg] in MX-80 and FEBEX bentonites after 1 and 6 months of interaction.

Experimental Cell	Distance from interface (mm)				
	1.5 mm	4.5 mm	10.5 mm	16.5 mm	19.5 mm
MX-80 reference	75 ± 4				
MX-80-1 month	63 ± 4	61 ± 6	76 ± 1	47 ± 10	65 ± 2
MX-80-6 months	80 ± 2	83 ± 2	74 ± 5	75 ± 8	72 ± 3
FEBEX reference	94 ± 1				
FEBEX-1 month	88 ± 3	89 ± 2	88 ± 3	89 ± 1	88 ± 1
FEBEX-6 months	74 ± 3	79 ± 3	86 ± 1	75 ± 1	81 ± 1

significant changes in chemical composition occurred mainly in the first mm of bentonite from the interface with steel (Fig. 4a-b). A well-defined altered zone was observed in the steel-bentonite contact, composed mainly by iron-rich corrosion products. The thickness of the alteration layer was heterogeneous (Fig. 4c). Averaged thicknesses of 50 to 250 µm were determined from the steel-MX-80 interface, after 1 and 6 months of reaction, respectively.

The bentonite side was enriched in Fe from the interface to a thickness of 0.8 mm after 1 month and up to 4 mm after 6 months (Fig. 5a-b). The concentration of Fe reached values >40 wt% over a thickness of 0.8–0.9 mm and then the concentration sharply decreased to values in the order of 10 wt%, as in the reference MX-80 bentonite. Higher values (>80 wt%) were only observed in a narrow zone of ~0.2 mm at the interface after 6 months, but the extension of the Fe enrichment (>15 wt %) reached up to 4 mm and then smoothly decreased to the original content of the unaltered reference bentonite. Accordingly, the relative concentration of Si and Al decreased in those zones enriched in Fe due to the presence of discrete patches of Fe corrosion products in this region.

The EDX analyses showed that Na, Mg and Ca decreased after 1 month near the interface with steel due to the presence of discrete filling of Fe corrosion products, however, after 6 months a relative increase in Mg was observed in a region between 0.2 and 1 mm (Fig. 5c-d). Below 0.2 mm, most of the montmorillonite was displaced and the area was occupied by the steel corrosion products, but in the region between 0.2 and 1 mm the chemical relative Mg concentrations increased from averaged 3 wt% to 7 wt%.

The averaged thicknesses of corrosion layer formed in the FEBEX bentonite, from the interface with steel, were 50 and 150 µm, after 1 and 6 months of interaction, respectively. This crust was mainly composed

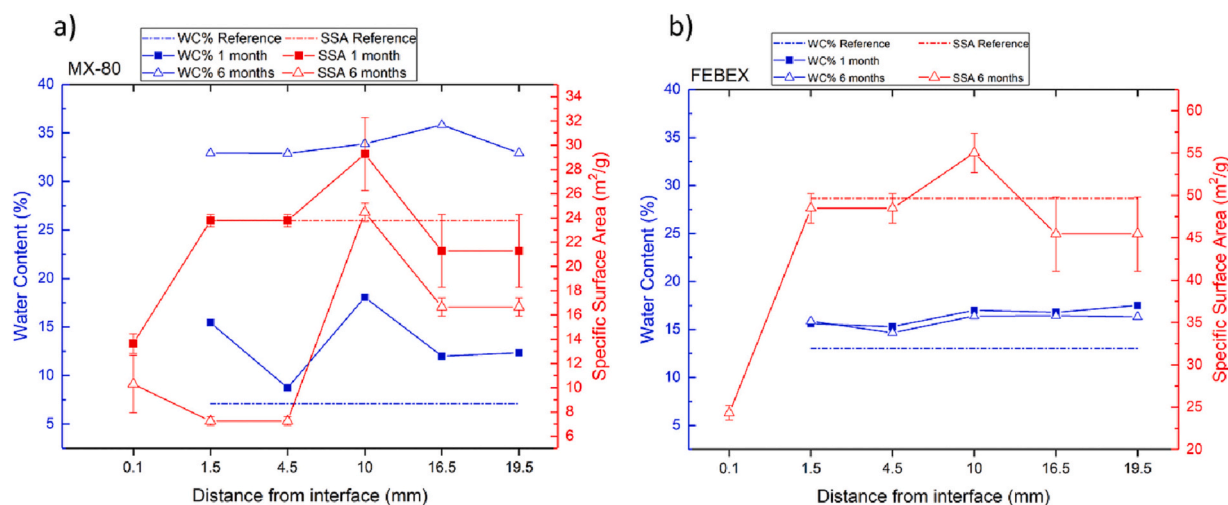


**Fig. 3.** Water content (left) and SSA (right) in bentonite as a function of the distance with the steel interface in a) MX-80 bentonite samples after 1 and 6 months; b) in FEBEX bentonite samples after 1 and 6 months (SSA after 1 month not shown). Reference values were measured on the original unreacted compacted bentonite (dotted lines).

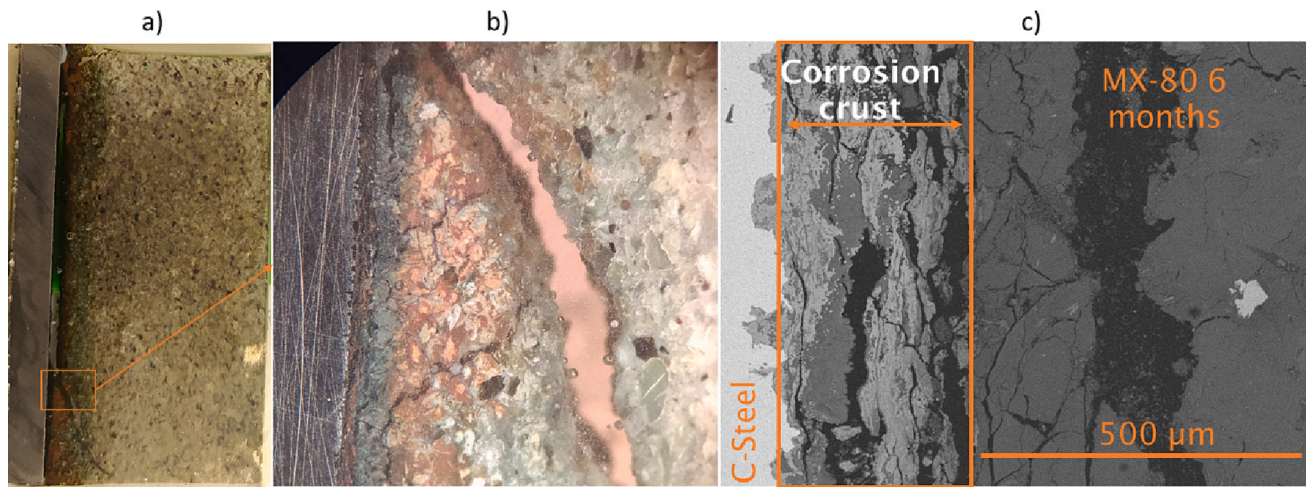


**Fig. 4.** Thin section of MX-80 after 6 months: a) aspect after cutting, resin embedding and polishing; b) aspect observed with the optical microscope; c) SEM image of the steel/bentonite interface.

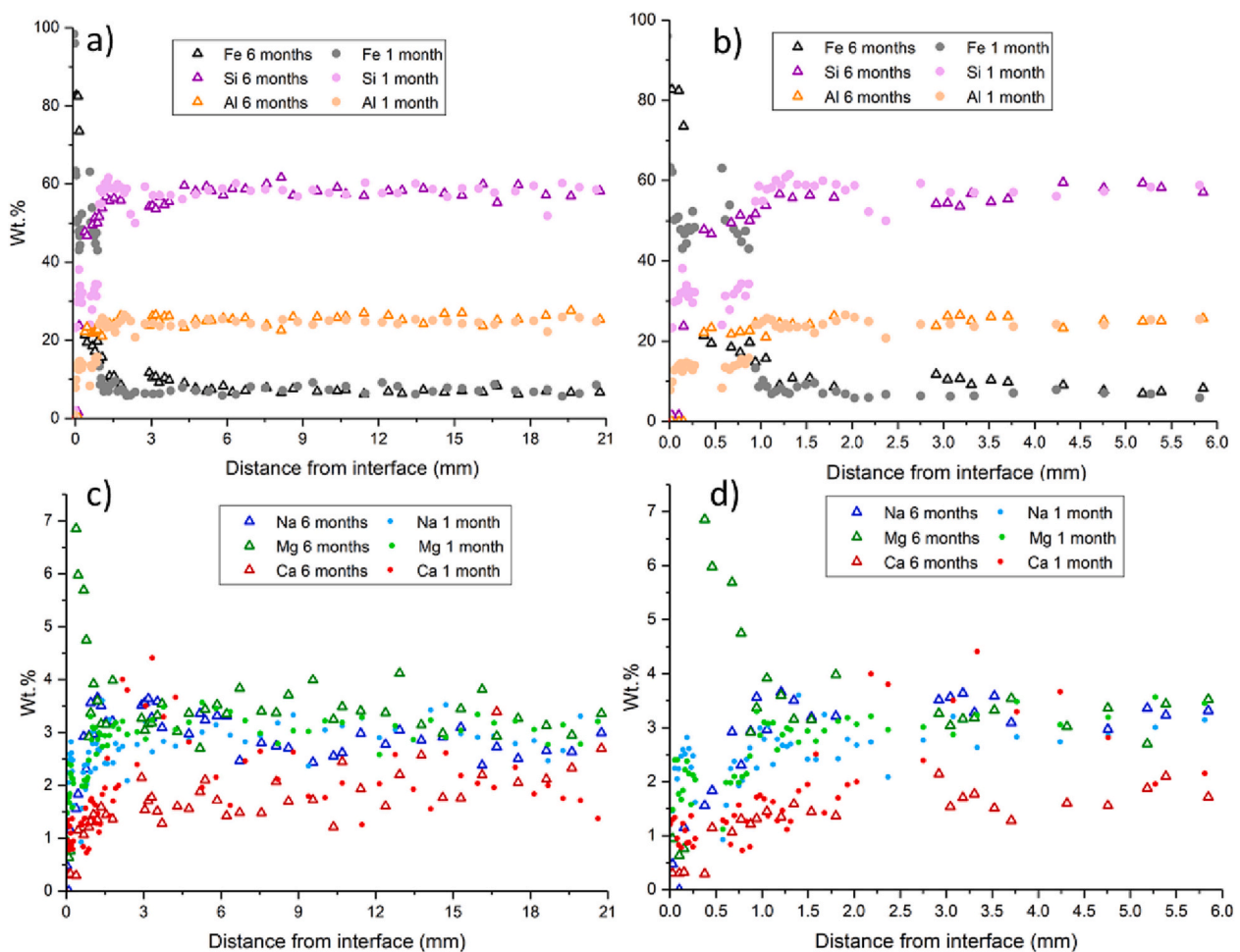


**Fig. 5.** EDX chemical profiles in MX-80 bentonite: a) EDX chemical composition of Fe, Si and Al expressed in wt% after 1 and 6 months. b) Detail of the EDX chemical composition over the first 6 mm; c) EDX chemical composition of Na, Mg and Ca expressed in wt% after 1 and 6 months; d) Detail of the EDX chemical composition over the first 6 mm.

by iron, as Si and Al decreased showing the iron corrosion products in that narrow zone. Bentonite close to the corrosion layer, high enrichment of Fe was observed up to ~1 mm after 1 month, coexisting with high relative concentrations of Si and Al. The Fe enrichment was less

concentrated but more extended in bentonite after 6 months (up to ~4 mm; Fig. 6a-b).

EDX analyses showed that Mg and Ca decreased after 1 month near the interface with the steel, however, after 6 months an increase of Mg



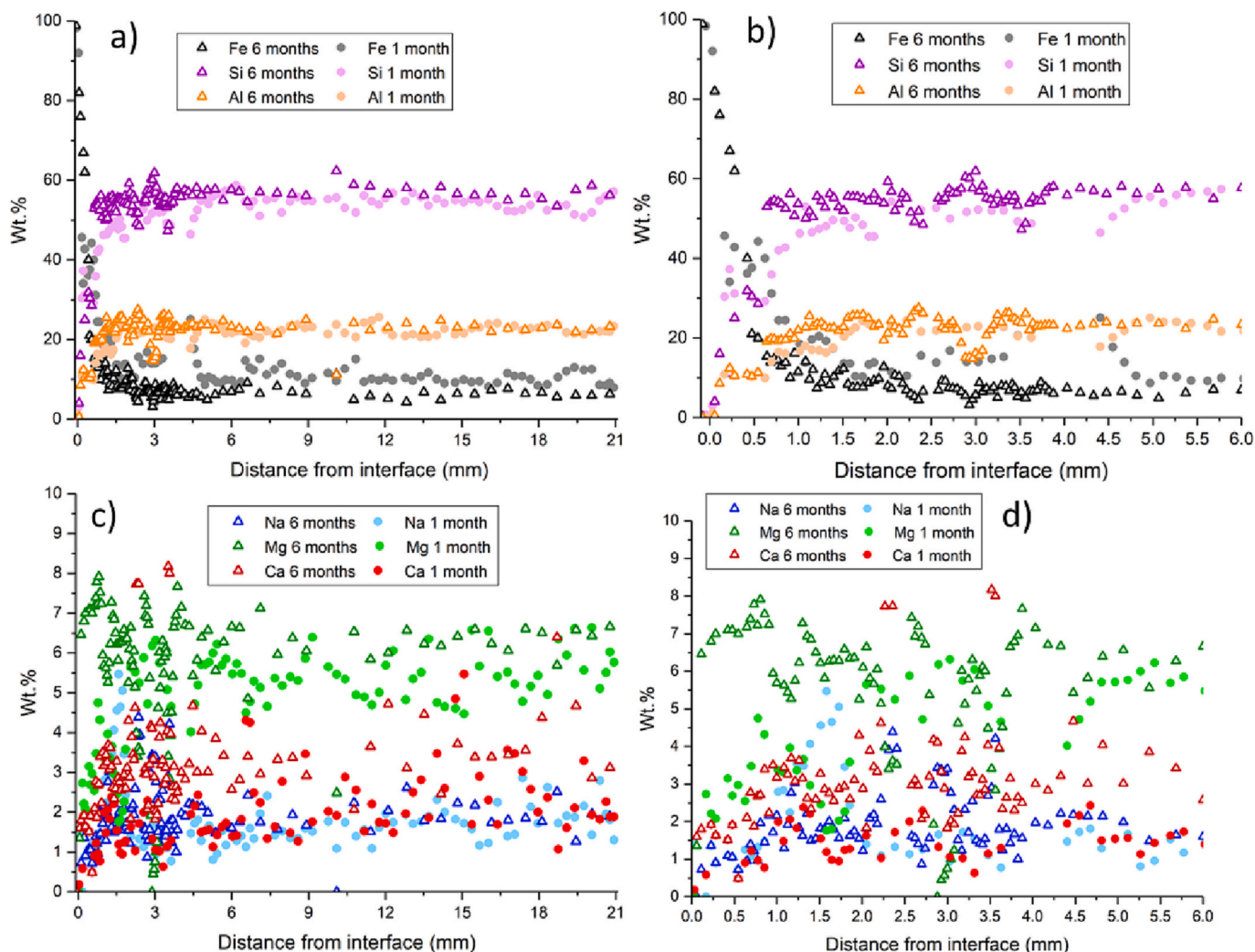


**Fig. 6.** EDX chemical profiles in FEBEX bentonite; a) EDX chemical composition of Fe, Si and Al expressed in wt% after 1 and 6 months; b) Detail of the EDX chemical composition over the first 6 mm; c) EDX chemical composition of Na, Mg and Ca expressed in wt% after 1 and 6 months. d) Detail of the EDX chemical composition over the first 6 mm.

was observed in a region between 0.15 and 1.5 mm (Fig. 6c-d). Likewise, Ca increased in a region between 0.15 and 4.5 mm after the corrosion layer. In this layer of 0.15 mm thickness, most of the observed material

corresponded to corrosion products mixed with bentonite. In the region between 0.15 and 1.5 mm the relative concentrations of Mg increased from an average of 3 wt% to 7.5 wt%. Ca and Mg increased along the

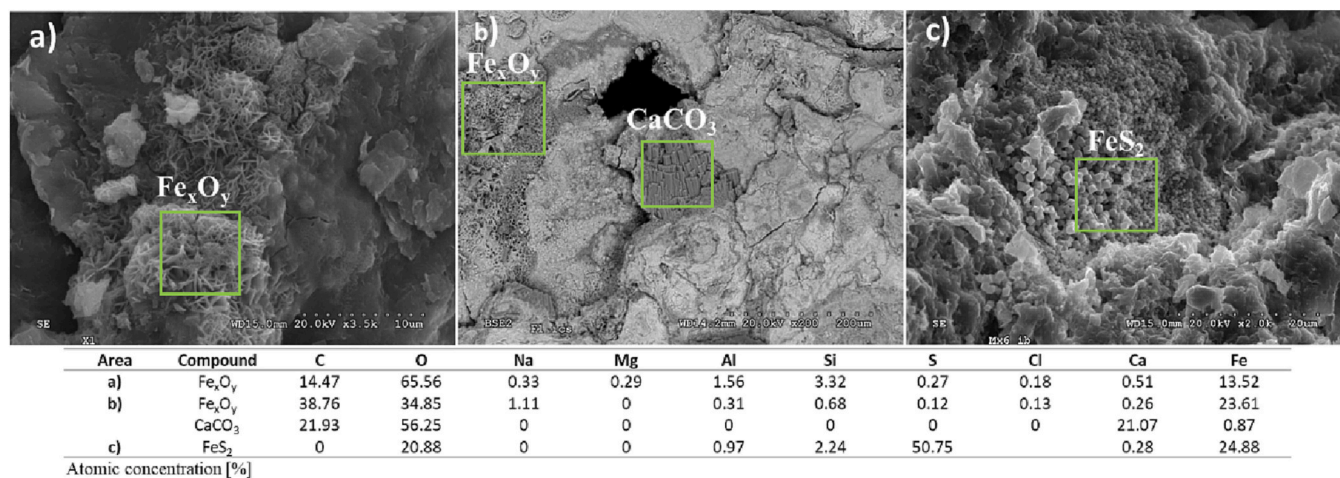


**Fig. 7.** SEM images of fragments of bentonite at the interface: a) Iron structures in MX-80 bentonite after 1 month; b) iron structures and CaCO<sub>3</sub> in FEBEX bentonite after 1 month; c) octahedral pyrite in MX-80 bentonite after 6 months.



bentonite block after 6 months.

EDX analyses in fresh fragments near the interface showed the presence of apparently new formed Fe-rich phases morphologies (Fig. 7a). FEBEX and MX-80 characteristic phases in the corrosion layer had different compositions. Despite of the presence of iron-rich

corrosion products, prismatic Ca-rich morphologies (presumably  $\text{CaCO}_3$  mineral) were frequently observed in experiments with FEBEX bentonite and octahedral pyrite in experiments with MX-80 bentonite (Fig. 7b and c). Fe enrichment on the clay surface was found in all four experiments, forming spicules structures with varying stoichiometries.

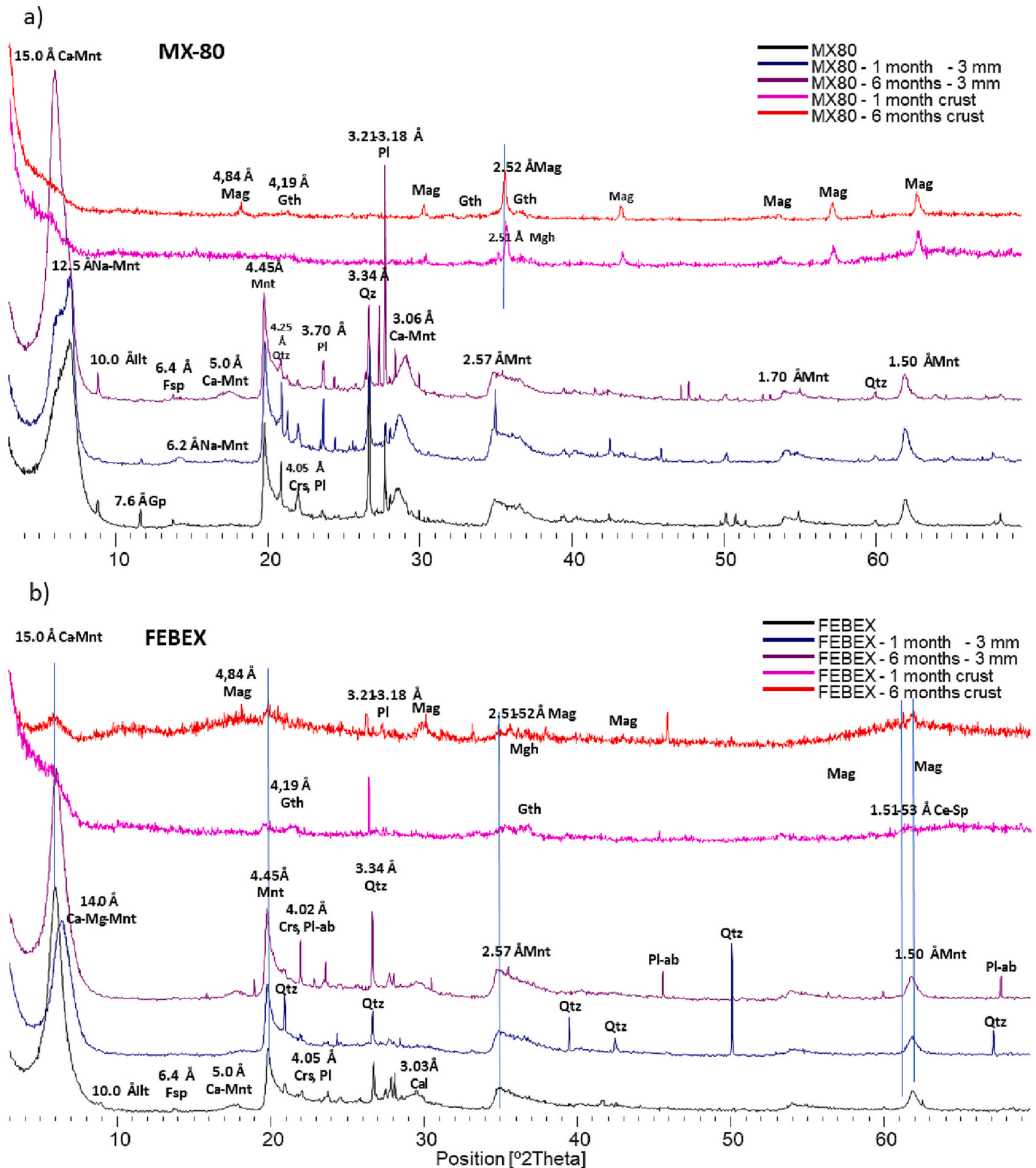


Fig. 8. Corrosion crust and bentonite in the 0–3 mm slice in contact with the steel plate: a) MX-80 experiments; b) FEBEX experiment. Ca-Mnt: calcium montmorillonite; Na-Mnt: sodium montmorillonite; Ill: illite; Gp: gypsum; Fsp: feldspars; Qtz: quartz; Cr<sub>2</sub>: cristobalite; Pl: plagioclase; Gth: goethite; Mag: magnetite; Mgh: maghemite; Ce: celadonite; sp.: saponite.

XRD analyses along the bentonite block showed minor alterations. The most significant alterations were found within the 3 mm closest to the interface with steel. The analyses were performed at the corrosion zone by direct exposition of the XRD beam to the corrosion surface after the steel plate and the bentonite were examined immediately after the corrosion crust. These compounds were found in a narrow zone at the steel-bentonite interface and were present in the form of a cemented crust of aggregates.

MX-80 bentonite changed from sodium to divalent calcium in the exchange complex as the basal spacing shifted from 12.5 to 15.0 Å after 6 months. Cristobalite was not detected after 6 months (4.05 Å reflection). Gypsum (7.6 Å reflection) decreased with time, disappearing after 6 months. Corrosion iron-rich crust exhibited disordered patterns with a high signal/noise ratio. The XRD pattern after 1 month showed maghemite-magnetite reflections. Small displacement and asymmetry towards the low angle side has been interpreted to indicate presence of maghemite. The XRD pattern after 6 months showed mainly magnetite and goethite as main Fe oxides (Fig. 8a).

The montmorillonite 001 reflection in FEBEX bentonite (Fig. 8b) showed a shift from 15 to 14 Å, comparing XRD pattern of the original sample with the interface sample (0–3 mm) after 1 month, but shifted again to 15 Å after 6 months, indicating the original montmorillonite character and presumably a larger Mg content after 1 month. This 14 Å reflection is not related to chlorite-like phases, that should present reflections at 7 and 3.5 Å, although chlorite XRD intensities may vary with Fe content. The 6 months pattern showed plagioclase reflections compared to the original sample, although in general there were no virtual variations in the shape and intensity of the broad reflections characterizing the predominant montmorillonite component. The FEBEX corrosion crust was highly disordered compared to MX-80. Broad reflections near the positions of reference magnetite-maghemite were identified. Goethite (4.19 Å) was present only in XRD pattern after 1 month. A high angle region, in the range of 61 to 63 2θ degrees, showed broad reflections that were not observed in MX-80. 1.50, 1.51 and 1.53 Å reflections were barely distinguished and indicated the transformation from di-octahedral (Al) to a Fe—Mg tri-octahedral 2:1 clay minerals in the FEBEX iron corrosion crust.

#### 4. Discussion

The design of the experiments has shown that the hydrothermal reaction at the carbon steel-bentonite interface can be studied as a function of time and is a valid technique to compare physico-chemical properties and the different response of alternative bentonites to be used in DGR for HLRW. The properties analysed showed different results as a function of time.

The water content increased in both bentonites, MX-80 and FEBEX, due to the imposed conditions of constant low pressure from the hydration side. In addition, the thermal gradient may have produced the mobilisation of water through the clay pores from the interface with the steel. Given the 100 °C temperature in the heater, water vapour could have formed and migrated through the porosity to condense in cooler areas (Villar et al., 2012). After 6 months of reaction the water content evolved differently between the MX-80 and FEBEX bentonites. A gradual increase in the water content occur for MX-80 and the bentonite might be saturated or near to complete saturation after 6, whereas the hydration process in the FEBEX bentonite has been fast over the first month, but then the water content remained in the same range over the next 5 months, presumably indicating that the complete saturation has been achieved earlier, although the water content is lower than in MX-80 or either that an unsaturated physical equilibrium stage was reached. Further results in longer term experiments (presently running) will help to confirm when the complete saturation is achieved.

The CEC decreased in both bentonites except for the region 0–6 mm from the interface with steel in MX-80 bentonite after 6 months. CEC decrease is normally related with montmorillonite dissolution or might

be associated to the modification of the crystal structure of montmorillonite particles near the steel interface. However, the decrease in the present study is not associated to any montmorillonite dissolution, as it was not observed by XRD. A decrease in CEC was also observed in FEBEX bentonite after 18 years of interaction with a C-steel heater at 100 °C in the in situ FEBEX experiment (Fernández et al., 2018b), and these authors attributed the effect to either increase of smectite layer charge, Fe<sup>III</sup>-bearing smectite reduction or collapse of clay particles caused by high salinity. Although the decrease in CEC was restricted to samples at very close contact with the C-steel heater. The CEC is also known to be dependant of pH. Larger pH lead to larger CEC values (Kaufhold and Dohrmann, 2013). These effects could have participated in the drop in CEC observed in this study, although the extension of any of them has not been quantified.

The decrease of the SSA close to the steel-bentonite interface was caused by the formation of corrosion products and mineralogical changes in the smectite structure. These changes were detected by SEM-EDX and XRD on samples at the interface, where magnetite, maghemite, and goethite precipitated as corrosion products. Other authors also included formation of hematite and lepidocrocite in similar systems (Carlson et al., 2007). The results obtained with XRD along the bentonite block indicated the partial conversion of Na-montmorillonite in MX-80 to a Ca-montmorillonite. This Ca could be provided by the dissolution of gypsum. The reduction in cristobalite indicated an alkaline dissolution process close to the interface (Kaufhold et al., 2013; Gómez-Espina and Villar, 2015; Kumpulainen et al., 2016), which might be in agreement with the accumulation of Mg in that zone (although pH could not be experimentally determined in that narrow zone), indicating either an alteration in the mineral chemistry or the precipitation of new Mg-rich mineral phases. Formation of magnesium silicate phases have been previously observed as a result of alkaline alteration bentonite, associated to a decrease of porosity (Fernández et al., 2018a). However, the pH conditions of the pore water in this narrow region close the steel interface cannot be confirmed in the present study.

The corrosion layer formed fast, but with increasing time the corrosion rate decreased in both bentonites. This could be by a protective effect that provided the initial corrosion layer. That crust limits the oxidation of deeper zones of the steel, slowing down the corrosion rate (Hadi et al., 2019). For this reason, the thickness of the corrosion layer after 6 months of interaction shows a thicker corrosion layer than after 1 month, but a lower corrosion rate than in the experiments after 1 month. Increase of Fe content in the montmorillonite structure could be explained by different pathways as suggested by Wersin et al. (2021), adsorbed at the interlayer by cation exchange, adsorbed at edge sites of the montmorillonite or at the corrosion products. In addition, redox reactions may have occurred with associated precipitation of Fe<sup>III</sup> oxides or mixed Fe<sup>II</sup>/Fe<sup>III</sup> oxides. Soluble Fe<sup>II</sup> migrates into the bentonite. The oxygen from the bentonite pores diffuses to the surface of the steel, when the iron meets the oxygen, it oxidises and precipitates on the montmorillonite surfaces as an iron (hydr)oxide as it is observed in Figs. 7 and 8.

The presence of maghemite in the samples could be explained by the oxidation of magnetite, which suggests that maghemite may be formed because of further oxidation of magnetite formed under reduced conditions during the experimental time. This could be caused by the separation of the samples from the carbon steel disc, which may have disrupted the electron transfer reaction between the solid Fe and the oxides. Also, this could be explained too by redox reactions that could occur during the sampling process by the oxidation in contact with oxygen (Zhao et al., 2019; Hiraga et al., 2021).

Presence of pyrite was observed only by SEM-EDX in MX-80 bentonite at the interface with the carbon steel. Its presence as a secondary mineral should imply highly reducing conditions or presence of sulphate reducing bacteria, able to reduce sulphates from the pore water. Activity of microorganisms at high temperatures are not considered and were not observed in bentonite samples in the in situ FEBEX experiment close to carbon steel heater (Bengtsson et al., 2017).

We could consider its presence as accessory mineral in the original sample, but the morphology observed by SEM-EDX indicated the coating of a clay surface rather than presence of single crystals that could occur as accessory minerals. Therefore, it might be plausible that pyrite precipitates as a result of local reducing conditions, but it cannot be confirmed.

## 5. Conclusions

The experimental system allowed to study the alteration of two compacted bentonites, interacting with a carbon steel, at a sub-mm scale, identifying the thickness and composition of the corrosion layer that formed at the interface and compare the different behaviour of two bentonites.

The hydrothermal gradient affected the specific surface area, the cation exchange capacity and the water content of both bentonites. During the first 6 months, the water content in MX-80 bentonite increased gradually and presumably became saturated while the FEBEX bentonite reached a similar water content after 1 and 6 months, although we cannot confirm the saturation state. Longer term experiments will confirm the water content evolution.

The steel-bentonite interaction caused a corrosion layer on the steel surface of varying thicknesses and favoured the enrichment of Fe in the bentonites. Irregular distributed corrosion thickness ranged from 50 to 250  $\mu\text{m}$ . MX-80 bentonite showed a thicker corrosion layer than FEBEX bentonite after six months of reaction. Magnetite, maghemite, hematite and goethite were identified as corrosion products. The presence of maghemite might have formed by the oxidation of magnetite during the dismantling or sampling. Pyrite presumably precipitated in MX-80 bentonite near the interface with steel, due to the availability of soluble Fe and  $\text{SO}_4^{2-}$  but that would require local reducing conditions that cannot be confirmed.

The presented study confirms the different reactivity of Na-bentonite and Ca-bentonite to the same system, as observed in larger scale experiments. A relative increase in Mg was observed in both bentonites at the interface with steel but, apart from an enrichment in the exchangeable region observed by XRD for the FEBEX bentonite after 1 month, that shift to Ca- enrichment after 6 months, no new mineral phases have been identified. Longer term experiments with both bentonites, presently under study, should bring light solve some uncertainties and better describe the temporal evolution.

## CRediT authorship contribution statement

**Carlos Mota-Heredia:** Methodology, Investigation, Data curation, Formal analysis, Writing – original draft. **Jaime Cuevas:** Conceptualization, Formal analysis, Supervision, Project administration, Funding acquisition, Writing – review & editing. **Ana I. Ruiz:** Investigation, Data curation. **Almudena Ortega:** Investigation, Resources. **Elena Torres:** Conceptualization. **María Jesús Turrero:** Conceptualization. **Raúl Fernández:** Conceptualization, Validation, Supervision, Project administration, Writing – review & editing.

## Declaration of Competing Interest

The authors declare that they have no known competing financial interests or personal relationships that could have appeared to influence the work reported in this paper.

## Data availability

Data will be made available on request.

## Acknowledgements

This manuscript has benefited from the comments and suggestion of

two anonymous reviewers and the editors, María Victoria Villar and Reiner Dohrmann. The authors acknowledge their contribution. This project has received funding from the European Union's Horizon 2020 research and innovation programme 2014-2018 under grant agreement N°847593.

## Appendix A. Supplementary data

Supplementary data to this article can be found online at <https://doi.org/10.1016/j.clay.2023.106984>.

## References

- Ammann, L., Bergaya, F., Lagaly, G., 2005. Determination of the cation exchange capacity of clays with copper complexes revisited. *Clay Miner.* 40, 441–453. <https://doi.org/10.1180/0009855054040182>.
- Beaucaire, C., Tertre, E., Ferrage, E., Grenut, B., Pronier, S., Madé, B., 2012. A thermodynamic model for the prediction of pore water composition of clayey rock at 25 and 80 °C — Comparison with results from hydrothermal alteration experiments. *Chem. Geol.* 334, 62–76. <https://doi.org/10.1016/j.chemgeo.2012.09.040>.
- Bengtsson, A., Blom, A., Taborowski, T., Schippers, A., Edlund, J., Kalinowski, B., Pedersen, K., 2017. FEBEX-DP: Microbiological Report (No. 16–15), Nagra Working Report.
- Bildstein, O., Claret, F., 2015. Chapter 5 - Stability of clay barriers under chemical perturbations. In: Fagpa, B. (Ed.), *Christophe Tournassat, C.I.S.I.C.B. Elsevier, Developments in Clay Science*, pp. 155–188. <https://doi.org/10.1016/B978-0-8100027-4.00005-X>.
- Bildstein, O., Trotignon, L., Perronnet, M., Jullien, M., 2006. Modelling iron-clay interactions in deep geological disposal conditions. *Phys. Chem. Earth Parts A/B/C* 31, 618–625.
- Bradbury, M.H., Baeyens, B., 2003. Porewater chemistry in compacted re-saturated MX-80 bentonite. *J. Contam. Hydrol.* 61, 329–338.
- Bradbury, M.H., Baeyens, B., 2009. Experimental and modelling studies on the pH buffering of MX-80 bentonite porewater. *Appl. Geochem.* 24, 419–425.
- Brookins, D.G., 1984. *Geochemical Aspects of Radioactive Waste Disposal*. Springer-Verlag, United States.
- Caballero, E., Fernandes Porto, M.J., Linares, J., Reyes, E., 1983. Mineralogy, geochemistry and mineral genesis of bentonites from Serrata de Nijar (Almería, Spain). *Estudios Geológicos (Madrid)* 39, 121–140.
- Caballero, E., Jiménez de Cisneros, C., Huertas, F.J., Huertas, F., Pozzuoli, A., Linares, J., 2005. Bentonite from Cabo de Gata, Almería, Spain: a mineralogical and geochemical overview. *Clay Miner.* 40, 463–480.
- Carlson, L., Karnland, O., Oversby, V.M., Rance, A.P., Smart, N.R., Snellman, M., Vähänen, M., Werme, L.O., 2007. Experimental studies of the interactions between anaerobically corroding iron and bentonite. *Phys. Chem. Earth Parts A/B/C* 32, 334–345. <https://doi.org/10.1016/j.pce.2005.12.009>.
- Chaparro, M.C., Finck, N., Metz, V., Geckeis, H., 2021. Reactive transport modelling of the long-term interaction between carbon steel and MX-80 bentonite at 25 °C. *Minerals* 11. <https://doi.org/10.3390/min11111272>.
- Chapman, N.A., 2006. Geological disposal of radioactive wastes – concept, status and trends. *J. Iber. Geol.* 32, 7–14.
- Cuevas, J., Cabrera, M.A., Fernández, C., Mota-Heredia, C., Fernández, R., Torres, E., Turrero, M.J., Ruiz, A.I., 2022. Bentonite Powder XRD Quantitative Analysis Using Rietveld Refinement: Revisiting and Updating Bulk Semiquantitative Mineralogical Compositions. *Minerals* 12, 772. <https://doi.org/10.3390/min12060772>.
- Cuevas, J., Ruiz, A.I., Fernández, R., Torres, E., Escribano, A., Regadío, M., Turrero, M.J., 2016. Lime mortar-compacted bentonite-magnetite interfaces: an experimental study focused on the understanding of the EBS long-term performance for high-level nuclear waste isolation DGR concept. *Appl. Clay Sci.* 124–125, 79–93. <https://doi.org/10.1016/j.clay.2016.01.043>.
- Edmunds, W., Savage, D., 1991. Geochemical characteristics of groundwater in granites and related crystalline rocks. In: *Applied Groundwater Hydrology*. Oxford University Press, pp. 266–282.
- El-Showk, S., 2022. Final resting place. *Science* 375, 806–810.
- ENRESA, 1997. *Evaluación del Comportamiento Y de la Seguridad de un Almacenamiento geológico Profundo en Granito (Publicación Técnica)*. ENRESA, Madrid.
- ENRESA (Ed.), 1998. *FEBEX. Bentonite: Origin, Properties and Fabrication of Blocks*, Publicación técnica 4/98. ENRESA, Madrid.
- Fernández, A.M., Baeyens, B., Bradbury, M., Rivas, P., 2004. Analysis of the porewater chemical composition of a Spanish compacted bentonite used in an engineered barrier. *Phys. Chem. Earth* 29, 105–118.
- Fernández, R., González-Santamaría, D., Angulo, M., Torres, E., Ruiz, A.I., Turrero, M.J., Cuevas, J., 2018a. Geochemical conditions for the formation of Mg silicates phases in bentonite and implications for radioactive waste disposal. *Appl. Geochem.* 93, 1–9. <https://doi.org/10.1016/j.apgeochem.2018.03.012>.
- Fernández, A.M., Kaufhold, S., Sánchez-Ledesma, D.M., Rey, J.J., Melón, A., Robredo, L. M., Fernández, S., Labajo, M.A., Clavero, M.A., 2018b. Evolution of the THC conditions in the FEBEX in situ test after 18 years of experiment: smectite crystallochemical modifications after interactions of the bentonite with a C-steel



- heater at 100 °C. *Appl. Geochem.* 98, 152–171. <https://doi.org/10.1016/j.apgeochem.2018.09.008>.
- Garraón, A., Gómez, P., Turrero, M.J., Torres, E., Buil, B., Sánchez, L., Peña, J., 2017. Hydrogeochemical Characterisation of the Groundwater in the FEBEX Gallery (Arbeitsbericht NAB No. NAB 16-14). NAGRA, Wettingen Switzerland.
- Gaucher, É.C., Blanc, P., Bardot, F., Braibant, G., Buschaert, S., Crouzet, C., Gautier, A., Girard, J.-P., Jacquot, E., Lassin, A., Negrel, G., Tournassat, C., Vinsot, A., Altmann, S., 2006. Modelling the porewater chemistry of the Callovian-Oxfordian formation at a regional scale. *Compt. Rendus Geosci.* 338, 917–930. <https://doi.org/10.1016/j.crte.2006.06.002>.
- Gautschi, A., 2017. Safety-relevant hydrogeological properties of the claystone barrier of a Swiss radioactive waste repository: an evaluation using multiple lines of evidence. *Grundwasser* 22, 221–233. <https://doi.org/10.1007/s00767-017-0364-1>.
- Gómez, P., Turrero, M.J., Garraón, A., Peña, J., Buil, B., de la Cruz, B., Sánchez, M., Sánchez, D.M., Quejido, A., Bajos, C., Sánchez, L., 2006. Hydrogeochemical characteristics of deep groundwaters of the Hesperian Massif (Spain). *J. Iber. Geol.* 32, 113–131.
- Gómez-Espina, R., Villar, M.V., 2010. Geochemical and mineralogical changes in compacted MX-80 bentonite submitted to heat and water gradients. *Appl. Clay Sci.* 47, 400–408. <https://doi.org/10.1016/j.clay.2009.12.004>.
- Gómez-Espina, R., Villar, M.V., 2015. Effects of heat and humidity gradients on MX-80 bentonite geochemistry and mineralogy. *Appl. Clay Sci.* 109–110, 39–48. <https://doi.org/10.1016/j.clay.2015.03.012>.
- Guillaume, D., Neaman, A., Cathelineau, M., Mosser-Ruck, R., Peiffert, C., Belmoula, M., Dubessy, J., Villieras, F., Michau, N., 2004. Experimental study of the transformation of smectite at 80 and 300 °C in the presence of Fe oxides. *Clay Miner.* 39, 17–34. <https://doi.org/10.1180/0009855043910117>.
- Hadi, J., Wersin, P., Serneels, V., Greneche, J.-M., 2019. Eighteen years of steel–bentonite interaction in the FEBEX in situ test at the Grimsel Test Site in Switzerland. *Clay Clay Miner.* 67, 111–131. <https://doi.org/10.1007/s42860-019-00012-5>.
- Hedin, A., 1997. Spent Nuclear Fuel. How Dangerous is it?, SKB Technical Report 97-13. Swedish Nuclear Fuel Waste Management Co., Stockholm, Swed.
- Hellä, P., Pitkänen, P., Löfman, J., Partamies, S., Vuorinen, U., Wersin, P., 2014. Safety Case for the Disposal of Spent Nuclear Fuel at Olkiluoto Definition of Reference and Bounding Groundwaters, Buffer and Backfill Porewaters (Report No. 2014-04), POSIVA 2014-04. POSIVA OY, Olkiluoto, Finland.
- Hiraga, R., da Fonseca, Otávio, Gomes, Martins, Neumann, R., 2021. Maghemite in Brazilian iron ores: quantification of the magnetite-maghemite isomorphic series by X-ray diffraction and the Rietveld method, and confirmation by independent methods. *Minerals* 11, 346. <https://doi.org/10.3390/min11040346>.
- IAEA, 2022. Status and Trends in Spent Fuel and Radioactive Waste Management, Nuclear Energy Series. International Atomic Energy Agency, Vienna.
- Jönsson, B., Åkesson, T., Jönsson, B., Meehdi, S., Janiak, J., Wallenberg, R., 2009. Structure and Forces in Bentonite MX-80, TR-09-06. Stockholm, Sweden.
- Kaufhold, S., Dohrmann, R., 2013. The variable charge of dioctahedral smectites. *J. Colloid Interface Sci.* 390, 225–233. <https://doi.org/10.1016/j.jcis.2012.09.023>.
- Kaufhold, S., Dohrmann, R., Sandén, T., Sellin, P., Svensson, D., 2013. Mineralogical investigations of the first package of the alternative buffer material test – I. Alteration of bentonites. *Clay Miner.* 48, 199–213. <https://doi.org/10.1180/claymin.2013.048.2.04>.
- Kaufhold, S., Hassel, A.W., Sanders, D., Dohrmann, R., 2015. Corrosion of high-level radioactive waste iron-canisters in contact with bentonite. *J. Hazard. Mater.* 285, 464–473. <https://doi.org/10.1016/j.jhazmat.2014.10.056>.
- Kaufhold, S., Dohrmann, R., Ufer, K., Kober, F., 2018. Interactions of bentonite with metal and concrete from the FEBEX experiment: mineralogical and geochemical investigations of selected sampling sites. *Clay Miner.* 53, 745–763. <https://doi.org/10.1180/clm.2018.54>.
- King, F., Shoesmith, D.W., 2010. 13 - Nuclear waste canister materials, corrosion behaviour and long-term performance in geological repository systems. In: Ahn, J., Apted, M.J. (Eds.), *Geological Repository Systems for Safe Disposal of Spent Nuclear Fuels and Radioactive Waste*. Woodhead Publishing, pp. 379–420. <https://doi.org/10.1533/9781845699789.3.379>.
- Kumpulainen, S., Kiviranta, L., Korkeakoski, P., 2016. Long-term effects of an iron heater and Äspö groundwater on smectite clays: chemical and hydromechanical results from the in situ alternative buffer material (ABM) test package 2. *Clay Miner.* <https://doi.org/10.1180/claymin.2016.051.2.02>.
- Laaksoharju, M., Tullborg, E.-L., Wikberg, P., Wallin, B., Smellie, J., 1999. Hydrogeochemical conditions and evolution at the Äspö HRL, Sweden. *Appl. Geochem.* 14, 835–859. [https://doi.org/10.1016/S0883-2927\(99\)00023-2](https://doi.org/10.1016/S0883-2927(99)00023-2).
- Lanson, B., Lantenois, S., van Aken, P.A., Bauer, A., Plançon, A., 2012. Experimental investigation of smectite interaction with metal iron at 80 °C: Structural characterization of newly formed Fe-rich phyllosilicates. *Am. Mineral.* 97, 864–871.
- Mäder, U., 2009a. Reference Pore Water for the Effingen Member (Standortregion Suidjura) for the Provisional Safety-Analysis in the Framework of the Sectoral Plan-Interim Results (SGT-ZE) (Arbeitsbericht NAB No. NAB 09-13). University of Bern, Institute of Geological Sciences.
- Mäder, U., 2009b. Reference Pore Water for the Opalinus Clay and “Bown Dogger” for the Provisional Safety-Analysis in the Framework of the Sectoral Plan-Interim Results (SGT-ZE) (No. NAB 09-14), Arbeitsbericht NAB. Nagra, Wettingen, Switzerland.
- Marsh, A.I., Williams, L.G., Lawrence, J.A., 2021. The important role and performance of engineered barriers in a UK geological disposal facility for higher activity radioactive waste. *Prog. Nucl. Energy* 137, 103736. <https://doi.org/10.1016/j.pnucene.2021.103736>.
- Martin, M., Cuevas, J., Leguey, S., 2000. Diffusion of soluble salts under a temperature gradient after the hydration of compacted bentonite. *Appl. Clay Sci.* 17, 55–70.
- Meier, L.P., Kahr, G., 1999. Determination of the cation exchange capacity (CEC) of clay minerals using the complexes of copper(II) ion with triethylenetetramine and tetraethylenepentamine. *Clay Clay Miner.* 47, 386–388.
- Montes-H, G., Fritz, B., Clement, A., Michau, N., 2005. Modelling of geochemical reactions and experimental cation exchange in MX80 bentonite. *J. Environ. Manag.* 77, 35–46.
- Mosser-Ruck, R., Cathelineau, M., Guillaume, D., Charpentier, D., Rousset, D., Barres, O., Michau, N., 2010. Effects of temperature, pH, and iron/clay and liquid/clay ratios on experimental conversion of dioctahedral smectite to berthierine, chlorite, vermiculite, or saponite. *Clay Clay Miner.* 58, 280–291. <https://doi.org/10.1346/ccmn.2010.0580212>.
- Mosser-Ruck, R., Sterpenich, J., Michau, N., Jodin-Caumon, M.-C., Randi, A., Abdelmoula, M., Barres, O., Cathelineau, M., 2020. Serpentinization and H<sub>2</sub> production during an iron-clay interaction experiment at 90C under low CO<sub>2</sub> pressure. *Appl. Clay Sci.* 191, 105609. <https://doi.org/10.1016/j.clay.2020.105609>.
- Navarro, V., Yustres, A., Asensio, L., De la Morena, G., González-Arteaga, J., Laurila, T., Pintado, X., 2017. Modelling of compacted bentonite swelling accounting for salinity effects. *Eng. Geol.* 223, 48–58. <https://doi.org/10.1016/j.enggeo.2017.04.016>.
- Necib, S., Linard, Y., Crusset, D., Michau, N., Daumas, S., Burger, E., Romaine, A., Schlegel, M.L., 2016. Corrosion at the carbon steel-clay borehole water and gas interfaces at 85 °C under anoxic and transient acidic conditions. *Corros. Sci.* 111, 242–258. <https://doi.org/10.1016/j.corsci.2016.04.039>.
- Necib, S., Diomidis, N., Keech, P., Nakayama, M., 2017. Corrosion of carbon steel in clay environments relevant to radioactive waste geological disposals, Mont Terri rock laboratory (Switzerland). *Swiss J. Geosci.* 110, 329–342. <https://doi.org/10.1007/s00015-016-0259-7>.
- Norris, S., 2017. Radioactive waste confinement: clays in natural and engineered barriers – introduction. *Geol. Soc. Lond., Spec. Publ.* 443, 1–8. <https://doi.org/10.1144/SP443.26>.
- NUMO, 2013. Safety of the Geological Disposal Project 2010 (Technical Report No. 13–05). NUMO, Tokyo, Japan.
- ONDRAF/NIRAS, 2013. Research, Development and Demonstration (RD&D) Plan for the Geological Disposal of High-Level and/or Long-Lived Radioactive Waste Including Irradiated Fuel if Considered as Waste. State-of-the-art report (Technical Report No. NIRONDF-TR 2013-12 E). Belgian Agency for Radioactive Waste and Enriched Fissile Materials, Belgium, Brussels, Belgium.
- Patel, R., Punshon, C., Nicholas, J., Bastid, P., Zhou, R., Schneider, C., Bagshaw, N., Howse, D., Hutchinson, E., Asano, R., King, S., 2012. Canister Design Concepts for Disposal of Spent Fuel and High Level Waste (No. NTB-12-06), Nagra Technical Report. Nagra, Wettingen (Switzerland).
- Pearson, F.J., Tournassat, C., Gaucher, E.C., 2011. Biogeochemical processes in a clay formation in situ experiment: part E – Equilibrium controls on chemistry of pore water from the Opalinus Clay, Mont Terri Underground Research Laboratory, Switzerland. *Appl. Geochem.* 26, 990–1008. <https://doi.org/10.1016/j.apgeochem.2011.03.008>.
- Ragvald, J., 2018. Hydrochemical Groundwater Monitoring Results from Water Sampling in the Forsmark Area 2016 (Report No. P-18-11), Hydrochemical Groundwater Monitoring. SKB.
- Rutqvist, J., 2020. Thermal management associated with geologic disposal of large spent nuclear fuel canisters in tunnels with thermally engineered backfill. *Tunn. Undergr. Space Technol.* 102, 103454. <https://doi.org/10.1016/j.tust.2020.103454>.
- SKB, 2006. Buffer and Backfill Process Report for the Safety Assessment SR-Can (No. TR-06-18), SKB Technical Report TR-06-18. Stockholm (Sweden).
- Smalios, E., Kienzler, B., 2005. Galvanic corrosion between the nuclear waste disposal container material pairs of copper-nickel alloys and carbon steel in salt brines. *Corrosion* 61, 230–236. <https://doi.org/10.5006/1.3280632>.
- Svensson, D., 2015. Saponite formation in the ABM2 iron-bentonite field experiment at Äspö hard rock laboratory, Sweden. In: Presented at the Clays in Natural and Engineered Barriers for Radioactive Waste Confinement, Sixth International Conference, Brussels, Belgium, pp. 168–169.
- Torres Álvarez, E., 2011. Procesos geoquímicos en la interfase acero al carbono/bentonita en un Almacenamiento Geológico Profundo: desarrollo experimental y modelización (Tesis Doctoral). Centro de Investigaciones Energéticas, Medioambientales y Tecnológicas (CIEMAT) Unidad de Barreras de Ingeniería y Geológicas.
- Turrero, M.J., Fernández, A.M., Peña, J., Sánchez, M.D., Wersin, P., Bossart, P., Sánchez, M., Melón, A., Garraón, A., Yllera, A., Hernán, P., Gómez, P., 2006. Pore water chemistry of a Paleogene continental mudrock in Spain and a Jurassic marine mudrock in Switzerland: sampling methods and geochemical interpretation. *J. Iber. Geol.* 32, 233–258.
- Villar, M.V., 2002. Thermo-Hydro-Mechanical Characterisation of a Bentonite from Cabo de Gata. A Study Applied to the Use of Bentonite as a Sealing Material in High Level Waste Repositories (Publicación Técnica No. 04–2002). ENRESA.
- Villar, M.V., Lloret, A., 2004. Influence of temperature on the hydro-mechanical behaviour of a compacted bentonite. *Appl. Clay Sci.* 26, 337–350.
- Villar, M.V., Martín, P.L., Bárcena, I., García-Siñeriz, J.L., Gómez-Espina, R., Lloret, A., 2012. Long-term experimental evidences of saturation of compacted bentonite under repository conditions. *Eng. Geol.* 149–150, 57–69. <https://doi.org/10.1016/j.enggeo.2012.08.004>.
- Villar, M.V., Gutiérrez-Álvarez, C., Martín, P.L., 2020. Low-suction water retention capacity of bentonite at high temperature. In: E3S Web of Conferences. Ciemat, p. 7. <https://doi.org/10.1051/e3sconf/202019504010>.

- Vinsot, A., Mettler, S., Wechner, S., 2008. In situ characterization of the Callovo-Oxfordian pore water composition. *Phys. Chem. Earth Parts A/B/C* 33, S75–S86. <https://doi.org/10.1016/j.pce.2008.10.048>.
- Wersin, P., Mazurek, M., Mäder, U.K., Gimmi, T., Rufer, D., Lerouge, C., Traber, D., 2016. Constraining porewater chemistry in a 250 m thick argillaceous rock sequence. *Chem. Geol.* 434, 43–61. <https://doi.org/10.1016/j.chemgeo.2016.04.006>.
- Wersin, P., Hadi, Jebril, Jenni, A., Svensson, D., Grenèche, Jean-Marc, Sellin, P., Leupin, O.X., 2021. Interaction of corroding iron with eight bentonites in the alternative buffer materials field experiment (ABM2). *Minerals* 11, 907. <https://doi.org/10.3390/min11080907>.
- Wilson, J., 2017. FEBEX-DP: Geochemical Modelling of Iron-Bentonite Interactions (No. QRS-1713A-R3 (v1.3)). Quintessa Ltd.
- Wilson, J.C., Benbow, S., Sasamoto, H., Savage, D., Watson, C., 2015. Thermodynamic and fully-coupled reactive transport models of a steel–bentonite interface. *Appl. Geochem.* 61, 10–28. <https://doi.org/10.1016/j.apgeochem.2015.05.005>.
- Zhao, J., Brugger, J., Pring, A., 2019. Mechanism and kinetics of hydrothermal replacement of magnetite by hematite. *Geosci. Front.* 10, 29–41. <https://doi.org/10.1016/j.gsf.2018.05.015>.